Charge- and spin-polarized currents in mesoscopic rings with Rashba spin-orbit interactions coupled to an electron reservoir

M. Ellner,[1] N. Bolívar,[1,2,3] B. Berche,[2,3] and E. Medina[1,2,3,*]

[1]*Escuela de Física, Facultad de Ciencias, Universidad Central de Venezuela, 1040 Caracas, Venezuela*

[2]*Groupe de Physique Statistique, Institut Jean Lamour, Université de Lorraine, 54506 Vandoeuvre-les-Nancy Cedex, France*

[3]*Centro de Física, Instituto Venezolano de Investigaciones Científicas, 21827, Caracas, 1020 A, Venezuela*

(Received 7 May 2014; revised manuscript received 24 July 2014; published 12 August 2014)

The electronic states of a mesoscopic ring are assessed in the presence of Rashba spin-orbit (SO) coupling and a U(1) gauge field. Spin-symmetric coupling to an ideal lead is implemented following Büttiker's voltage probe. The exact density of states is derived using the reservoir uncoupled eigenstates as basis functions mixed by the reservoir coupling. The decay time of uncoupled electron eigenstates is derived by fitting the broadening profiles. Spin and charge persistent currents are computed in the presence of the SO interaction and the reservoir coupling for two distinct scenarios of the electron filling fraction. The degradation of the persistent currents depends uniformly on the reservoir coupling but nonuniformly in temperature, the latter due to the fact that currents emerge from different depths of the Fermi sea, and thus for some regimes of flux, they are provided with a protective gap. Such flux regimes can be tailored by the SO coupling for both charge and spin currents.

DOI: 10.1103/PhysRevB.90.085305 PACS number(s): 68.65.La, 73.23.Ra, 72.25.Dc, 03.65.Yz

I. INTRODUCTION

Recently, there has been a growing interest in the spin-orbit (SO) interaction, partly due to its omnipresence in noncentrosymmetric semiconductors with high technological value such as GaAs, InSb, and CdTe, all with a zinc-blende structure [1]. It is of special interest that the Rashba spin-orbit interaction (RSOI) may be used to implement control of the spin degree of freedom through electrical means [2] since spin more weakly couples to decoherence effects as compared to the charge [3]. In particular, spin-asymmetric mesoscopic rings combine well-known charge interference effects with spin-orbit interactions, that cause spin splitting and spin interference [4,5] even in the absence of a magnetic field, while preserving time-reversal symmetry. Such a combination of interactions plus the existence of edges, give rise to the spin quantum Hall effect and topological insulators [6]. These novel states of matter have many new potential applications radiating from the fact that conduction states are protected against impurity scattering.

Recent proposals, based on spin-orbit controlled spin precession in mesoscopic rings or interferometric devices, cover many mechanisms for generating spin-polarized electrons by electric and magnetic flux control [7–11] and charge and spin currents driven by electromagnetic pulses [12]. Graphene-based materials for rings are also promising, due to the possibility of substrate interactions [13] or intercalating atoms [14] that have been devised to enhance an otherwise weak Rashba spin-orbit coupling.

In this work, we study the effects of a voltage probe coupling and temperature effects on the coherence of spin-split bands in a Rashba coupled ring. The experimental realization of the ring is generally understood to be within a two-dimensional (2D) electron gas, where the Rashba coupling is induced by the structural inversion asymmetry through a gate voltage. Nevertheless, this same gate can be a source of dephasing as electrons couple to it as a voltage probe. The robustness of any proposed device must measure up to the effects of the environment. A particularly simple model, for analytical treatment, is the Büttiker probe model [15], extensively used in the literature [16–19]. An emblematic phase-coherent phenomenon used as a testing ground is that of persistent charge and spin currents, the latter made possible by the RSO coupling. We determine the persistent charge and spin currents in a 2D electron gas built into a mesoscopic ring with narrow confinement [8,20]. RSO interaction is contemplated as arising from structural inversion asymmetry built into the electron potential controlled by a gate. The solution to this problem in the completely coherent limit has been addressed before both in the continuum Hamiltonian [5,8,11,20,21] and the tight-binding version [22]. We briefly revisit the problem in the continuum, to derive the basis functions, in order to address the exact solution to the voltage-probe model [15] including SO active media. While the uncoupled ring is diagonalizable as a Hamiltonian problem, the reservoir coupling is formulated in the scattering formalism. The coupling of these two problems, generalizing Büttiker's treatment, allows us to obtain analytical expressions for the densities of states and equilibrium currents from the quantum mechanical definitions.

We compute the decay of persistent currents with the coupling to the electron reservoir and also with temperature, determined solely by effect of the Fermi distribution. For low enough temperatures, we find that charge and spin persistent currents exhibit robust oscillations, following the uncoupled spectrum of the ring and their magnitude can be controlled by the external magnetic flux (up to $0.5h/e$ through the ring). The spin current can be made to switch signs and stay constant at constant magnitude quite robustly. While strong cancellation of the contributions to charge and spin currents is still generic in the presence of RSO coupling, we find that there are ranges in flux where currents are thermally protected by a gap. These ranges can be tuned by the SO coupling.

*Corresponding author: ernestomed@gmail.com

II. STATES OF THE DECOUPLED SO ACTIVE RING

The two-dimensional quantum Hamiltonian for electrons of effective mass m^* is given by [4,23]

$$H = \frac{\mathbf{\Pi}^2}{2m^*} + \alpha\,(\boldsymbol{\sigma} \times \mathbf{\Pi}) + U(\boldsymbol{r}), \tag{1}$$

were σ_i are the Pauli matrices, $\mathbf{\Pi} = (\boldsymbol{p} - e\boldsymbol{A})$, and $U(\boldsymbol{r})$ defines the confinement potential of a ring geometry. α is the coupling strength of the Rashba spin-orbit interaction $\tilde{V}_R$, tunable by an external electric field, and A_i are the components of the vector potential associated with an external magnetic field in the $\hat{z}$ direction. It is assumed that only the ground-state radial mode of the potential $U(\boldsymbol{r})$ is involved. The treatment and role of higher-order radial model has been addressed in Ref. [20].

A straightforward "classical" coordinate change of this Hamiltonian $(x,y) \to (\rho,\phi)$ results in a non-Hermitian form that must be symmetrized appropriately. The correct Hermitian RSO potential in polar coordinates is given by the usual coordinate transformation plus a basis rotation of the spinor [24]

$$V_R = e^{i\sigma_z\frac{\varphi}{2}}\tilde{V}_R e^{-i\sigma_z\frac{\varphi}{2}} = -\hbar\omega_{\mathrm{SO}}\sigma_\rho\left(i\partial_\varphi + \frac{\Phi}{\Phi_0}\right) - i\hbar\frac{\omega_{\mathrm{SO}}}{2}\sigma_\varphi, \tag{2}$$

where $\omega_{\mathrm{SO}} = \frac{\alpha}{r_0}$, r_0 is the ring radius, and $\Phi_0 = 2\pi\hbar/e$ is the quantum of flux. The rotated Pauli matrices are defined as $\sigma_\varphi = -\sigma_x\sin\varphi + \sigma_y\cos\varphi$ and $\sigma_\rho = \sigma_x\cos\varphi + \sigma_y\sin\varphi$. Adding the kinetic energy operator reads the Hamiltonian

$$H = \hbar\Omega\left(i\frac{\partial}{\partial\varphi} + \frac{\Phi}{\Phi_0}\right)^2 - \hbar\omega_{\mathrm{SO}}\sigma_\rho\left(i\frac{\partial}{\partial\varphi} + \frac{\Phi}{\Phi_0}\right) - i\frac{\hbar\omega_{\mathrm{SO}}}{2}\sigma_\varphi, \tag{3}$$

with $\Omega = \hbar/2mr_0^2$. Completing squares taking into account operator ordering and the angular dependencies of σ_φ and σ_ρ, one arrives at the compact form

$$H = \hbar\Omega\left(-i\frac{\partial}{\partial\varphi} - \frac{\Phi}{\Phi_0} + \frac{\omega_{\mathrm{SO}}}{2\Omega}\sigma_\rho\right)^2 - \frac{\hbar\omega_{\mathrm{SO}}^2}{4\Omega}. \tag{4}$$

In order to obtain the eigenvalues, we can focus only on the quadratic term, and restore the additive scalar term to the resulting eigenvalue. We can then solve the simpler eigenvalue equation

$$\left(-i\frac{\partial}{\partial\varphi} - \frac{\Phi}{\Phi_0} + \frac{\omega_{\mathrm{SO}}}{2\Omega}\sigma_\rho\right)\psi = \sqrt{\frac{E}{\hbar\Omega}}\psi. \tag{5}$$

Clearly ψ, a spinor, is also an eigenfunction of the square of the previous operator with the square of the eigenvalue. The proposed form for the eigenspinor is

$$\psi_j^\mu(\varphi) = e^{in_j^\mu\varphi}\chi^\mu(\varphi) = e^{in_j^\mu\varphi}\begin{pmatrix} A^\mu \\ e^{i\varphi}B^\mu \end{pmatrix}, \tag{6}$$

where j labels right and left propagating plane waves ($j = 1$ clockwise and $j = 2$ counterclockwise), μ is the spin label, and $n_j^\mu \in \mathbb{Z}$ ($\mu = 1$ spin up and $\mu = 2$ spin down). Solving the matrix equation, the eigenvalues are found to be [25]

$$E_{n,j}^\mu = \hbar\Omega\left((-1)^j n - \frac{\Phi}{\Phi_0} + \frac{1}{2\pi}\Phi_{\mathrm{AC}}^{(\mu)}\right)^2 - \frac{\hbar\omega_{\mathrm{SO}}^2}{4\Omega}, \tag{7}$$

where $\Phi_{\mathrm{AC}} = \pi(1 + (-1)^\mu\sqrt{1 + (\omega_{\mathrm{SO}}/\Omega)^2})$ (AC for Aharonov-Casher phase). The eigenfunction coefficients satisfy the relation

$$\frac{\Omega}{\omega_{\mathrm{SO}}}\left(1 + (-1)^\mu\frac{1}{\cos\theta}\right)A^\mu = B^\mu, \tag{8}$$

with $\cos\theta = 1/\sqrt{1 + (\omega_{\mathrm{SO}}/\Omega)^2}$. One can then choose $A^{(1)} = B^{(2)} = \cos\frac{\theta}{2}$ and $-A^{(2)} = B^{(1)} = \sin\frac{\theta}{2}$. We thus arrive at the eigenfunctions

$$\psi_j^1(\varphi) = e^{in_j^1\varphi}\begin{pmatrix} \cos\frac{\theta}{2} \\ e^{i\varphi}\sin\frac{\theta}{2} \end{pmatrix}, \qquad \psi_j^2(\varphi) = e^{in_j^2\varphi}\begin{pmatrix} \sin\frac{\theta}{2} \\ -e^{i\varphi}\cos\frac{\theta}{2} \end{pmatrix}, \tag{9}$$

where $\frac{\theta}{2} = \tan^{-1}[\Omega/\omega_{\mathrm{SO}} - \sqrt{(\Omega/\omega_{\mathrm{SO}})^2 + 1)}]$. Figure 1 shows the spectrum for $\omega_{\mathrm{SO}}/\Omega = 0.75$. The spin-orbit interaction preserves time-reversal symmetry, so in the absence of a magnetic field $E_{n,+}^\uparrow = E_{n,-}^\downarrow$, i.e., twofold degeneracies. On applying a magnetic flux, this degeneracy is broken, but it is restored at half integer flux quanta. For zero SO coupling and in the absence of a Zeeman term, there is a peculiar twofold degeneracy for each level due to the closing of the wave function for half-integer spin [26]. Thus, $E_{n,-}^\uparrow = E_{n+1,-}^\downarrow$ and $E_{n,+}^\downarrow = E_{n+1,+}^\uparrow$ for all fluxes. At zero and half-integer flux quanta, we have fourfold degeneracy in the absence of SO coupling. Such degeneracies are important when computing the corresponding charge and spin currents. The wave functions in Eqs. (9) form a complete four-function basis we will use to represent the voltage-probe coupled system.

III. DECOHERENCE WITH SPIN-ORBIT COUPLING

In Ref. [15], Büttiker introduced an ingenious way to couple a simple quantum system (a ring) to a reservoir that behaved like a voltage probe (zero current condition to reservoir). This model leads to a variety of generalizations [27]. The approach here is similar; as the coupling to the reservoir is not defined in Hamiltonian terms and leads to dephasing, we have a Hamiltonian solution to the uncoupled problem and a scattering approach for the coupling to the reservoir. The two problems meet by writing the new wave functions as a superposition of the uncoupled ring basis functions with coefficients determined by matching boundary conditions. Coupling to the reservoir is introduced in a ring through an ideal lead that acts as a voltage probe (no net current threads the lead). The reservoir emits electrons with a Fermi distribution.

The coupling between the lead and the ring is described by the scattering matrix S, which relates the incoming and outgoing amplitudes $\vec{\alpha}' = S\vec{\alpha}$. The current conservation implies that S is unitary. The matrix is 3×3 for each spin label μ as the coupling to the reservoir is spin symmetric. In

general, the matrix S will have five independent parameters. Considering S to be symmetric with respect to the two branches of the ring, the number of independent parameters reduces to three:

$$S = \begin{pmatrix} r_{33} & t_{32} & t_{31} \\ t_{23} & r_{22} & t_{21} \\ t_{13} & t_{12} & r_{11} \end{pmatrix} = \begin{pmatrix} -(a+b) & \sqrt{\varepsilon} & \sqrt{\varepsilon} \\ \sqrt{\varepsilon} & a & b \\ \sqrt{\varepsilon} & b & a \end{pmatrix}, \quad (10)$$

where $a = (\sqrt{1-2\varepsilon}-1)/2$, $b = (\sqrt{1-2\varepsilon}+1)/2$, and ε is the coupling parameter with the reservoir, which varies between 0 and $\frac{1}{2}$ corresponding to going from the uncoupled to the maximally coupled limits [28]. We have also written the S matrix in terms of $t_{i,j}$, the transmission amplitude between the ith and jth leads (see Fig. 2) and $r_{i,i}$ the reflection amplitude back into the same lead i, with $i = 1,2,3$, where 3 refers to the reservoir lead and 1,2 to the ring, either left or the right to the reservoir lead. The symmetry of the terms in the S matrix, referred to this formulation, depends on which fields are present, as we will see in the following.

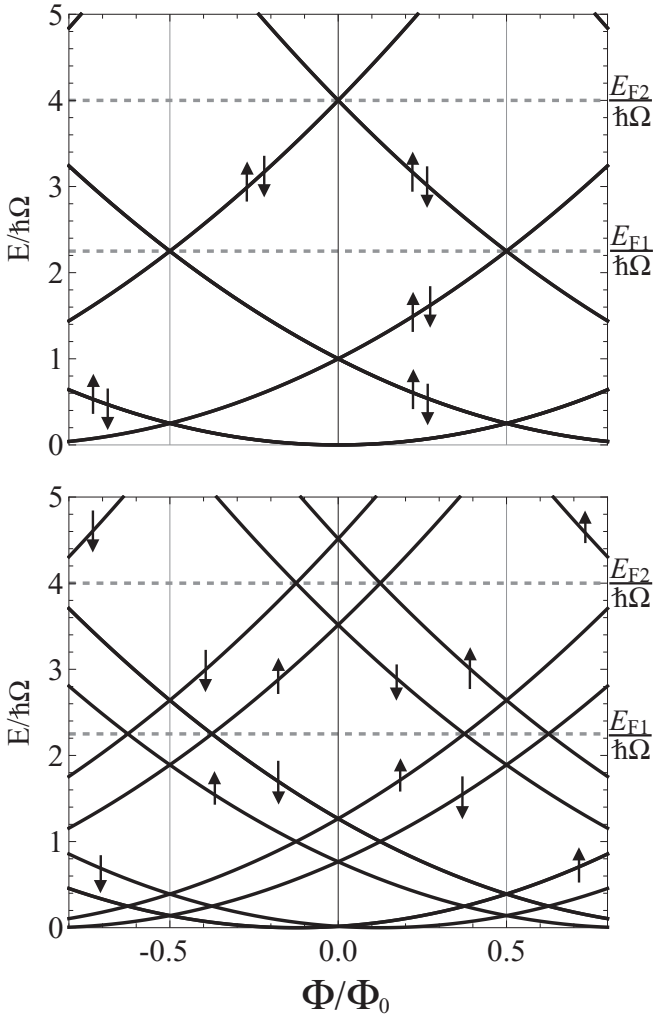

FIG. 1. Energy states of the decoupled ring for $\omega_{SO}/\Omega = 0$ (top) and $\omega_{SO}/\Omega = 0.75$ (bottom). The two dashed lines represent Fermi levels considered to compute the charge and spin currents. The breaking of spin degeneracy, on applying SO coupling, allows for equilibrium spin currents.

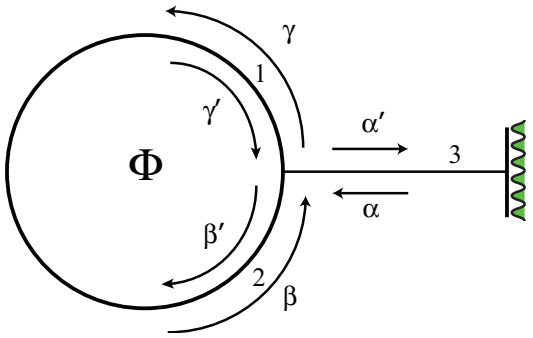

FIG. 2. (Color online) Modeled ring configuration threaded by a magnetic flux depicting reservoir lead 3 and ring leads 1 and 2. The greek labels encode the wave-function amplitudes, as explained in the text.

The lead coupling the ring to the reservoir needs two equivalent spin channels and can thus be expanded as

$$\psi_{\text{lead}}(x) = \sum_{\mu=1,2} \phi_{\text{lead}}(x)\chi^{(\mu)}(0), \qquad x \in (-\infty, 0] \quad (11)$$

where x is the coordinate along the lead and $x = 0$ is defined as the coordinate at which the lead connects to the ring, while the reservoir is at $x = -\infty$, and χ^{μ} is a two-component spinor eigenstate of σ_z. As the reservoir lead is not spin-orbit active, its energies are $E = \hbar^2 k^2/2m$. The coefficients of the expansion in Eq. (11) are given by

$$\phi_{\text{lead}}(x) = \sqrt{\mathcal{N}}(e^{ikx} + C_3 e^{-ikx}). \quad (12)$$

The normalization prefactor is determined following Büttiker's argument: in an energy interval $E, E + dE$, the differential of current injected into the lead is $dI = ev(dN/dE)f(E)dE$, where $f(E)$ is the Fermi distribution, $dN/dE = 1/2\pi\hbar v$ is the density of states of a perfect lead, and $v = \hbar k/m$. The wave function for the lead contemplates the correct current if $\mathcal{N} = f(E)dE/2\pi\hbar v$.

The ring wave function is now a mixture of the four basis functions of the uncoupled case, so that we may accommodate for the new boundary conditions. We define

$$\Psi(\varphi) = C_1^1\psi_1^1(\varphi) + C_1^2\psi_1^2(\varphi) + C_2^1\psi_2^1(\varphi) + C_2^2\psi_2^2(\varphi), \quad (13)$$

where coefficients are to be fixed by imposing equality of the wave functions at $x = 0$ for $\varphi = 0$ and 2π. The scattering problem is written as $\vec{\alpha}'^{(\mu)} = S\vec{\alpha}^{(\mu)}$, the coefficients $\vec{\alpha}^{(\mu)} = (\alpha^{(\mu)}, \beta^{(\mu)}, \gamma^{(\mu)})$ and $\vec{\alpha}'^{(\mu)} = (\alpha'^{(\mu)}, \beta'^{(\mu)}, \gamma'^{(\mu)})$ are found evaluating (12) at the junction at $x = 0$ (see Fig. 2) for $\alpha^{(\mu)}$ and $\alpha'^{(\mu)}$, and evaluating ψ_2^{μ} at $\varphi = 0, 2\pi$ for the $\beta'^{(\mu)}$ and $\gamma^{(\mu)}$, respectively. Finally, the coefficients $\beta^{(\mu)}$ and $\gamma'^{(\mu)}$ are found evaluating ψ_1^{μ} at $\varphi = 0, 2\pi$, respectively. The set of equations can be cast, for each spin subspace, as

$$\begin{pmatrix} \sqrt{\mathcal{N}}C_3^{\mu} \\ C_1^{\mu} \\ C_2^{\mu} \end{pmatrix} = \begin{pmatrix} -(a+b) & \sqrt{\varepsilon} & \sqrt{\varepsilon}e^{2\pi i n_1^{\mu}} \\ \sqrt{\varepsilon} & a & be^{2\pi i n_1^{\mu}} \\ \sqrt{\varepsilon}e^{-2\pi i n_2^{\mu}} & be^{-2\pi i n_2^{\mu}} & ae^{-2\pi i(n_1^{\mu}-n_2^{\mu})} \end{pmatrix} \begin{pmatrix} \sqrt{\mathcal{N}} \\ C_2^{\mu} \\ C_1^{\mu} \end{pmatrix}, \quad (14)$$

where we have absorbed the phase factors into a redefined S matrix that manifestly displays the symmetry of the system. Note that we can invert for the quantum number as a function of the energy and fields

$$n_j^\mu = (-1)^j \sqrt{\frac{E}{\hbar\Omega}} + \frac{\Phi}{\Phi_0} - \frac{1}{2}\left(1 + (-1)^\mu \sqrt{1 + \left(\frac{\omega_{\rm SO}}{\Omega}\right)^2}\right). \tag{15}$$

Referring to Eq. (10), one can readily check that, in the absence of magnetic or SO fields, $t_{jk} = t_{kj} = \sqrt{\varepsilon} e^{2\pi i n_1^\mu} = \sqrt{\varepsilon} e^{-2\pi i n_2^\mu}$, i.e., S is an orthogonal (symmetric) matrix, time-reversal invariant. When the magnetic field is on but there is no SO coupling, then $t_{jk} \neq t_{kj}$ so $n_1^\mu \neq n_2^\mu$ and time-reversal symmetry is broken. When the magnetic field is turned off and the SO coupling is present, time-reversal symmetry is restored, and there is the additional symmetry for changing j and μ labels simultaneously. Thus, the larger 6×6 matrix $S \otimes \mathbb{1}_s$ matrix is symplectic and embodies Kramers degeneracy. Solving the system of equations, one can obtain each of the amplitudes

$$\begin{aligned}
C_1^\mu &= \frac{\sqrt{\epsilon\mathcal{N}}\left(1 - e^{2\pi i n_2^\mu}\right)}{\left(1 - be^{2\pi i n_1^\mu}\right)\left(b - be^{2\pi i n_2^\mu}\right) + a^2\left(1 - be^{2\pi i n_1^\mu}\right)}, \\
C_2^\mu &= \frac{\sqrt{\epsilon\mathcal{N}}\left(e^{2\pi i n_1^\mu} - 1\right)}{\left(1 - be^{2\pi i n_1^\mu}\right)\left(b - be^{2\pi i n_2^\mu}\right) + a^2\left(1 - be^{2\pi i n_1^\mu}\right)}, \\
C_3^\mu &= \frac{\epsilon\left[e^{2\pi i n_1^\mu} - 1 + \left(1 - e^{2\pi i n_2^\mu}\right)e^{2\pi i n_1^\mu}\right]}{\left(1 - be^{2\pi i n_1^\mu}\right)\left(b - be^{2\pi i n_2^\mu}\right) + a^2\left(1 - be^{2\pi i n_1^\mu}\right)} \\
&\quad - (a + b).
\end{aligned} \tag{16}$$

For the charge density, the modulus squared of the coefficients acquires a particularly simple form in terms of the coupling parameters,

$$\left|C_1^\mu\right|^2 = \frac{2\varepsilon\mathcal{N}}{g^{(\mu)}}\left[1 - \cos\left(2\pi n_2^\mu\right)\right], \tag{17}$$

$$\left|C_2^\mu\right|^2 = \frac{2\varepsilon\mathcal{N}}{g^{(\mu)}}\left[1 - \cos\left(2\pi n_1^\mu\right)\right], \tag{18}$$

$$|C_3^\mu|^2 = 1, \tag{19}$$

where

$$\begin{aligned}
g^{(\mu)} &= 3 + \sqrt{1 - 2\varepsilon} - 3\varepsilon - 2(1 + \sqrt{1 - 2\varepsilon} - \varepsilon) \\
&\quad \times \cos\left(2\pi n_1^\mu\right) + 2\sqrt{1 - 2\varepsilon}\cos\left(2\pi\left(n_1^\mu - n_2^\mu\right)\right) \\
&\quad - 2\cos\left(2\pi n_2^\mu\right) + \cos\left[2\pi\left(n_1^\mu + n_2^\mu\right)\right] + (\sqrt{1 - 2\varepsilon} - \varepsilon) \\
&\quad \times \left\{-2\cos\left(2\pi n_2^\mu\right) + \cos\left[2\pi\left(n_1^\mu + n_2^\mu\right)\right]\right\}.
\end{aligned} \tag{20}$$

Note the very important character of the model expressed in Eq. (19); the lead amplitude has modulus one, thus two opposite propagating waves superpose to give a constant amplitude, which means there is no net current (voltage-probe condition) to or from the reservoir.

For the density of states (DOS) we know that the number of electrons in the energy interval dE is given by $dN = |C_1^1|^2 + |C_1^2|^2 + |C_2^1|^2 + |C_2^2|^2$. As each amplitude modulus is proportional to the energy interval dE and using the chain rule $dN/dk = (dN/dE)(dE/dk) = (dN/dE)\hbar^2 k/m$, the number of electrons per unit energy range is given by

$$\frac{dN}{dE} = \sum_{i,\mu} \frac{\varepsilon f(E)}{\pi\hbar v} \frac{\left(1 - \cos 2\pi n_i^\mu\right)}{g^{(\mu)}}, \tag{21}$$

so, expanding the sum in Eq. (21) and using the chain rule, the DOS can be written as

$$\begin{aligned}
\frac{dN}{dk} &= \frac{2\varepsilon}{\pi}\left(\frac{\sin^2\left(2\pi n_1^1\right) + \sin^2\left(2\pi n_2^1\right)}{g^{(1)}}\right. \\
&\quad \left. + \frac{\sin^2\left(2\pi n_1^2\right) + \sin^2\left(2\pi n_2^2\right)}{g^{(2)}}\right).
\end{aligned} \tag{22}$$

The explicit relation between DOS and energy comes from substituting here the expressions for n_j^μ in Eq. (15) for the uncoupled problem. Equation (15) now defines this quantum number which becomes a continuous function of the energy, flux, and SO coupling, and is no longer restricted to be integer or half-integer as the problem is now coupled, through the wave-function amplitudes, to the reservoir.

The limit of zero fields (neither SO nor magnetic field) with coupling to the reservoir recovers Büttiker's result [15]

$$\frac{dN}{dk} = \frac{4\varepsilon\cos^2\left(2\pi\sqrt{\frac{E}{\hbar\Omega}}\right)}{\pi\left[-1 + \varepsilon + \sqrt{1 - 2\varepsilon}\cos\left(2\pi\sqrt{\frac{E}{\hbar\Omega}}\right)\right]}. \tag{23}$$

Figure 3 shows the DOS for $\varepsilon \neq 0$. The levels increasingly broaden around the quantized energies of the decoupled ring ($\varepsilon = 0$) as ε increases. The uncoupled quantized values correspond to the poles of the density of states at zero coupling, which obey the relation $E = n^2\hbar\Omega$, with n an integer (values $n^2 = 0, 1, 4, \ldots$ in the figure). When the coupling is turned on, one expects that the levels are shifted to lower energies as they broaden from self-energy corrections due to the reservoir [29]. Deeper levels appear less coupled (broaden less) to the reservoir than the shallower counterparts.

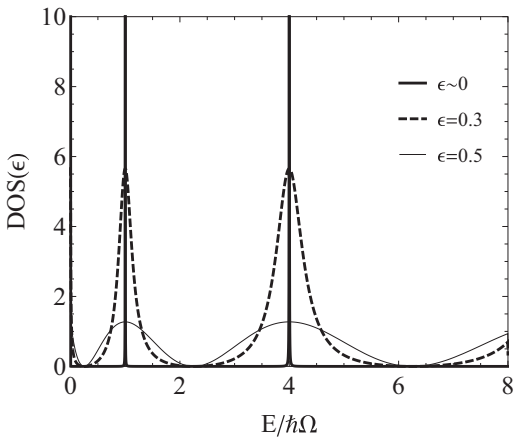

FIG. 3. Density of states on the ring as a function of the energy for two values of the coupling parameter of the reservoir and $T = 0$. ($\omega_{\rm SO}/\Omega = 0$, $\Phi/\Phi_0 = 0$.) The energy is expressed in units $E_0 = \hbar\Omega$.

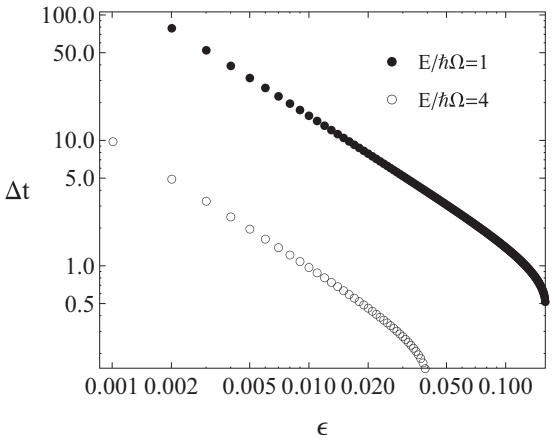

FIG. 4. Lifetime of the electrons in the ring as a function of the coupling to the reservoir ε. The energies correspond to the quantized values of the decoupled states. The time is given in atomic units 1 a.u. $\approx 2.4 \times 10^{-17}$ s.

A simple analysis of the poles reveals some of the aforementioned features to lowest order in ε. For the case without SO and zero magnetic field, the pole of Eq. (23) is at

$$\frac{E_n}{\hbar\Omega} = n^2 - \frac{\varepsilon^2}{4\pi^2} + i\frac{n}{\pi}\varepsilon(1+\varepsilon) + \mathcal{O}(\varepsilon^3), \qquad (24)$$

where the n dependence comes from the condition $n = (1/2\pi)\cos^{-1}(1)$. Note the downshift of the real part of the energy proportional to ε^2 as expected, and an energy broadening (imaginary part) with linear and quadratic contributions in the reservoir coupling. Additionally, the broadening is proportional to the principal quantum number n, so that the peaks broaden more as the energy increases.

Making a correspondence between level broadening and electron lifetime, by fitting the resonance to a Lorentzian form, leads to Fig. 4. From Eq. (24) one obtains $\Delta t = \pi/[2\Omega n\varepsilon(1+\varepsilon)] = \pi/(2\Omega n\varepsilon) - \pi/(2\Omega n) + \pi\varepsilon/(2\Omega n) + \ldots$. The power law coming from the dominant term is $\propto\varepsilon^{-1}$ independent of the n. This reproduces the behavior of Fig. 4 for small couplings to the reservoir. Only the regime where the broadening is reasonably Lorentzian is taken into account. As can be seen from the figure, the broadening function becomes nontrivial for $\varepsilon > 0.1$, where the power-law decay changes. One subtle fact about the resonance position is that it does not depend on the reservoir coupling, the resonances are always positioned according to $E_n/\hbar\Omega = n^2$. This is due to the behavior of the numerator of the density of states close to the polar values. In this sense, this resonance is not conventional.

In spite of the smearing of the energy levels, which one generally associates with increased uncertainty of the energies, we recall that even in the reservoir coupled case, we always know the full wave function. So, the treatment is always fully coherent, and no information is lost. Uncertainty of the states derives from accounting only for part of the wave function (see expression for the number of states dN) which lives on the ring and forgetting about the amplitude leaking into the cable towards the reservoir.

In order to see that the values of ε are reasonable for a real experimental ring attached to a reservoir (see Table I for a summary of parameters considered), we propose a simple potential barrier coupling generated by a gate voltage. Taking the WKB approximation for the transmission probability $\mathcal{T}$ we can estimate $\varepsilon \sim \sqrt{\mathcal{T}} = 4(E/V_0)(1 - E/V_0)\exp[-(2m^*/\hbar^2)^{1/2}(V_0 - E)^{1/2}L]$. Reasonable values for the parameters are $V_0 = 0.1$ eV for the barrier height, $L = 5$ nm for the barrier length, semiconductor effective mass of $m^* = 0.042m$ (m the bare electron mass) with a ring radius $r_0 = 50$ nm (to estimate the ring Fermi energy). For the two Fermi energies considered E_{F_1} ~0.54 meV and E_{F_2} ~1 meV, we get values of $\varepsilon \sim 0.06$–0.08 for a weakly coupled ring. To increase ε, one adjusts the barrier height or length.

TABLE I. Typical values for parameters and physical quantities used in this work.

Range of parameters	Normalization
Effective mass of electrons	
$m^* = 0.042m$	
Ring radius	
$r_0 = 100$ to 300 nm	
Fermi energies	
$E_{F_1} = 2.25\hbar\Omega$ to $4\hbar\Omega$	$\Omega = \hbar/2mr_0^2$
Magnetic field flux	
$\Phi = 0$ to $0.5\Phi_0$	$\Phi_0 = h/\lvert e\rvert$
SO coupling	
$\omega_{SO} = 0$ to $1.25\,\Omega$	$\Omega = \hbar/2mr_0^2$
Coupling to reservoir	
$\epsilon = 0$ to 0.5	Dimensionless
Temperature scale	
$T = 0$ to $0.5\,T_0$	$T_0 = \hbar^2/2mk_Br_0^2$
Charge current	
$J_q = 0$ to $4\,J_0$	$J_0 = \hbar^2/2mr_0^2\Phi_0$
Spin current	
$J_s = 0$ to $3\,J_0$	$J_0 = \hbar^2/2mr_0^2$

The magnetic field shifts the states and the SO coupling breaks the twofold degeneracy as was discussed. Figure 5 shows the effect of the magnetic field and the SO coupling, respectively, on the DOS. In the top panel, each peak is doubly degenerate, while this degeneracy is broken with SO as depicted in the bottom panel. The values assumed for the RSO, e.g., $\omega_{SO}/\Omega = 0.75$ corresponds to $\hbar\alpha \sim 3.02 \times 10^{-12}$ eV m, a realistic value for GaAs [30]. This degeneracy can appear to exist when the coupling to the reservoir is sufficiently large [see Fig. 5(b)] for $\varepsilon = 0.5$, as the DOS broadens into a single peak containing both levels.

IV. PERSISTENT CHARGE CURRENTS

For a decoupled ring at zero temperature, the charge persistent currents can be calculated by the linear-response relation [24,31] $J_q = -\sum_i \frac{dE_i}{d\Phi}$ where i encompasses the occupied states. The leading contributions to the current, due to cancellation of current contributions from state with opposite slopes, are the states close to the Fermi level. The linear-response relation is not useful when the ring is coupled to the reservoir since the energies broaden into a continuum of levels. On the other hand, we have derived the exact wave functions from which the current may be determined by the

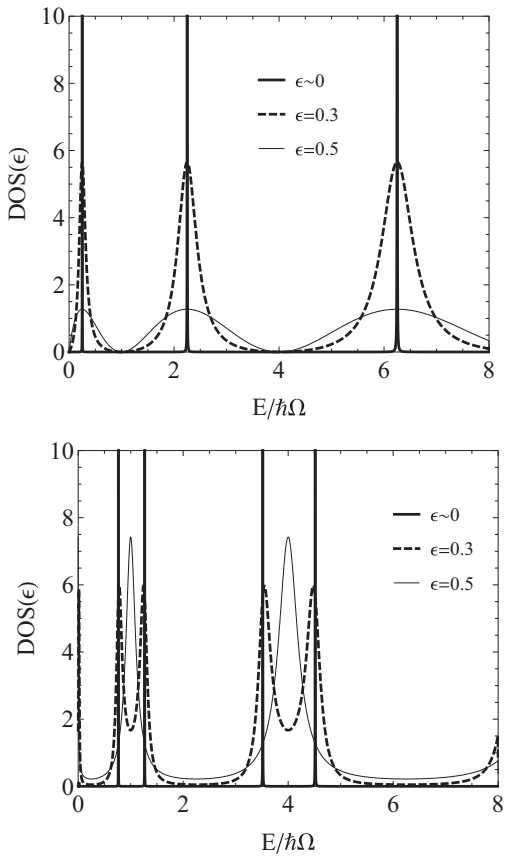

FIG. 5. Density of states of the ring as a function of the energy for three values of ε and $T = 0$. The values of the parameters are $\omega_{SO}/\Omega = 0$ (top panel) and $\Phi/\Phi_0 = 0.5$ and $\omega_{SO}/\Omega = 0.75$, $\Phi/\Phi_0 = 0$ for the bottom panel.

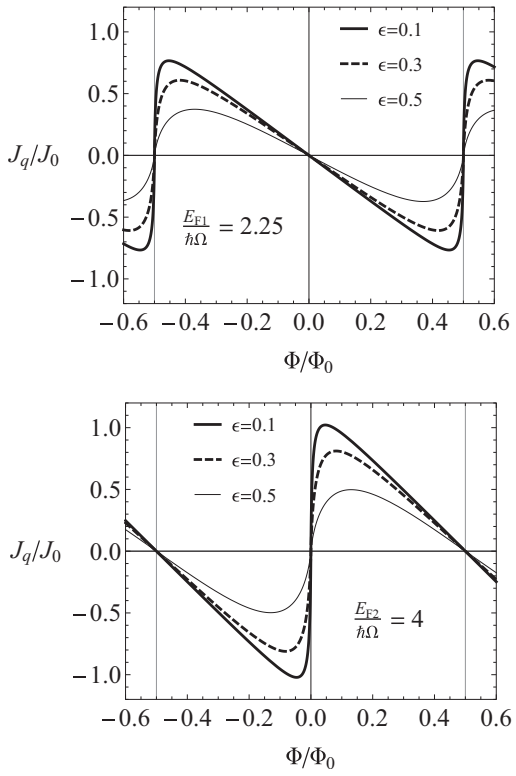

FIG. 6. Charge persistent current as a function of the magnetic flux for three values of the reservoir coupling parameter. The number of electrons is 6 (top) and 8 (bottom) corresponding to a Fermi energy of E_{F_1} and E_{F_2}, respectively (see Fig. 1). The RSO interaction is off and the persistent current is given in units $J_0 = \hbar\Omega/\Phi_0$.

expectation value of the charge current operator $\Psi^\dagger e v_\varphi \Psi$ where

$$v_\varphi = r_0\dot{\varphi} = (r_0/i\hbar)[\varphi, H] = -2r_0\Omega\left(-i\frac{\partial}{\partial\varphi} - \frac{\Phi}{\Phi_0} + \frac{\omega_{SO}}{2\Omega}\sigma_\rho\right). \quad (25)$$

Integrating over all occupied states up to the Fermi level including the electron occupation numbers, one obtains

$$J_q = -\frac{2\varepsilon\hbar\Omega}{\Phi_0}\sum_{m,\mu}\int\frac{dE}{\hbar\Omega}\frac{f(E)}{\sqrt{\frac{E}{\hbar\Omega}g^\mu}}\sin^2\left(\pi n_m^\mu\right) \times\left[n_{\overline{m}}^\mu - \frac{\Phi}{\Phi_0} + \delta^\mu\right], \quad (26)$$

with

$$\delta^1 = \sin^2\frac{\theta}{2} + \frac{\omega_{SO}}{2\Omega}\sin\theta; \quad \delta^2 = \cos^2\frac{\theta}{2} - \frac{\omega_{SO}}{2\Omega}\sin\theta, \quad (27)$$

where $\overline{m}$ is the complement value of m. The natural current scale is identified as $J_0 = \hbar\Omega/\Phi_0$. Note that $\varepsilon = 0$ does not imply zero current [15] (in fact it is largest at zero coupling) as g^μ also depends on the coupling with a nontrivial limit behavior. We will separate the discussion into two cases: (i) The Fermi level fixes $N = 6$ electrons (see Fig. 6 top panel), corresponding to E_{F_1} in Fig. 1, and (ii) $N = 8$ (see Fig. 6 bottom panel) corresponding to E_{F_2} in Fig. 1. In the absence of RSO interaction for the first case, there are two electrons, one with spin up and the other with spin down, at each energy. At the Fermi level, two bands which describe electrons with different propagation numbers j cross each other at half-integer steps in Φ_0 (see Fig. 1). This results in a jump in the sign of the current at these values. In the second case, the levels cross at zero or integer flux quanta, and the sign jump occurs at those points. These are the behaviors expected also for small couplings to the reservoir. Figure 6 shows the charge currents without the SO coupling as a function of the magnetic field. The reduction in amplitude of the current as a function of the reservoir coupling strength is evident. For Fermi level E_{f_1}, the persistent current is minimal for the smallest fluxes and gradually grows, while for E_{f_2} the current is maximal at the smallest fluxes and decreases thereof.

After including RSO, the crossing between bands at the Fermi level shifts to $\Phi/\Phi_0 = m/2 + [1 \pm \sqrt{1 + (\omega_{SO}/\Omega)^2}]/2$, with $m \in \mathbb{Z}$ for the case (i) and $\Phi/\Phi_0 = m/2 \pm \sqrt{1 + (\omega_{SO}/\Omega)^2}/2$ for case (ii) displacing the current jumps and introducing two more for each of the Fermi-level scenarios [32] (see Fig. 7). The current jumps from $|\Phi/\Phi_0| < 0.5$ have a smaller amplitude at finite RSO because the levels in the latter case are nondegenerate, and cause only half of the full current jump amplitude at $|\Phi/\Phi_0| = 0.5$.

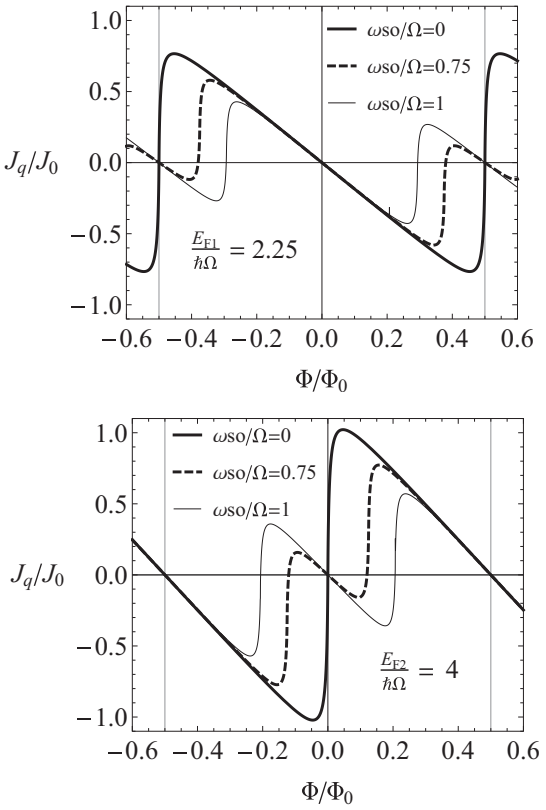

FIG. 7. Charge persistent current as a function of the magnetic flux for different RSO values. The reservoir coupling is $\varepsilon = 0.1$. The number of electrons is 6 (top) and 8 (bottom) corresponding to a Fermi energy of E_{F_1} and E_{F_2} according to Fig. 1.

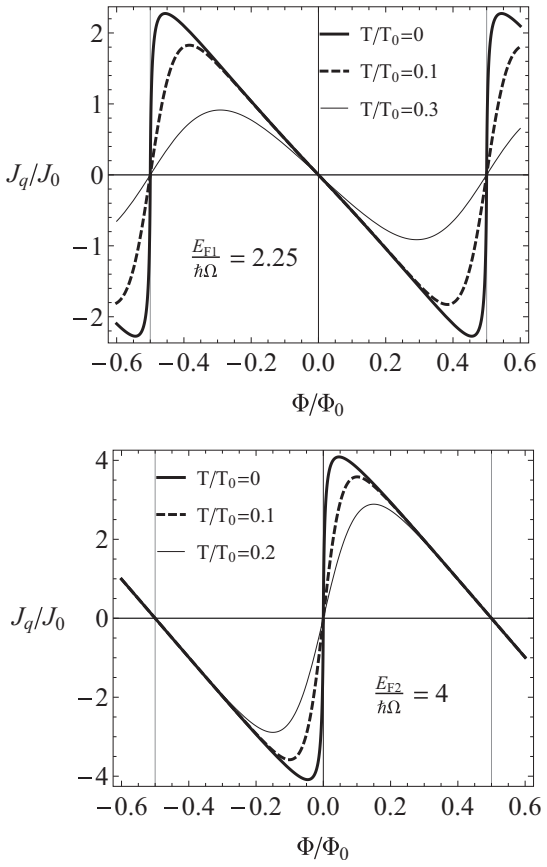

FIG. 8. Charge persistent current as a function of the magnetic flux and no SO coupling, for different temperatures, for a fixed $\varepsilon = 0.1$ and referred to the scale $T_0 = \hbar\Omega/k_B$. The number of electrons is 6 (top) and 8 (bottom). Note the low sensitivity of the current to thermal effects when current arises from below the Fermi levels.

The degradation of current with temperature has a distinctive character as compared to the coupling to the reservoir, as can be seen in Fig. 8. The temperature effect will be small when the current emanates from a level appreciably below the Fermi level, so that few electrons are actually promoted to counter current states. On the other hand, for fluxes where the currents arise from levels close to the Fermi level, the currents quickly degrade. For the case where currents originate from within the Fermi sea, there is a gap protecting persistent currents that is energy dispersion dependent. See Refs. [26,33] where currents are protected from thermal effects by a linear dispersion.

Figure 9 shows the dependence of charge current on temperature, for different ring-reservoir couplings. For certain selected ranges of the magnetic flux, the persistent current can be degraded completely. Otherwise, there is always a remanent charge current. We estimate the magnitude of the thermal effects by using the temperature scale $T_0 = \hbar\Omega/k_B$. As Ω depends on the size of the ring, $T/T_0 = 0.5$ in the figures correspond to temperatures between 526 and 59 mK for ring sizes between 100 and 300 nm and an effective mass of $m^* = 0.042m$. This implies that the gap for persistent current degradation is of the order of 40 μeV for the smallest of the rings. Improving this gap with either effective mass or ring radius and flux point of operation, should improve the thermal robustness of high-sensitivity cantilevers [34] for noise and electron thermometry.

V. PERSISTENT SPIN CURRENTS

In order to compute the spin currents, we use the standard definition through the anticommutator between the velocity

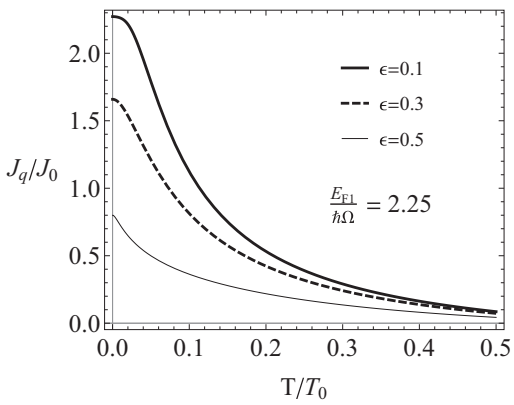

FIG. 9. Temperature dependence of the charge current for the scenario of E_{F_1} and no SO coupling. Depending on the magnetic flux chosen (here chosen $\Phi/\Phi_0 = -0.46$ but the scenario is valid in a vicinity of this flux), the current can be degraded completely.

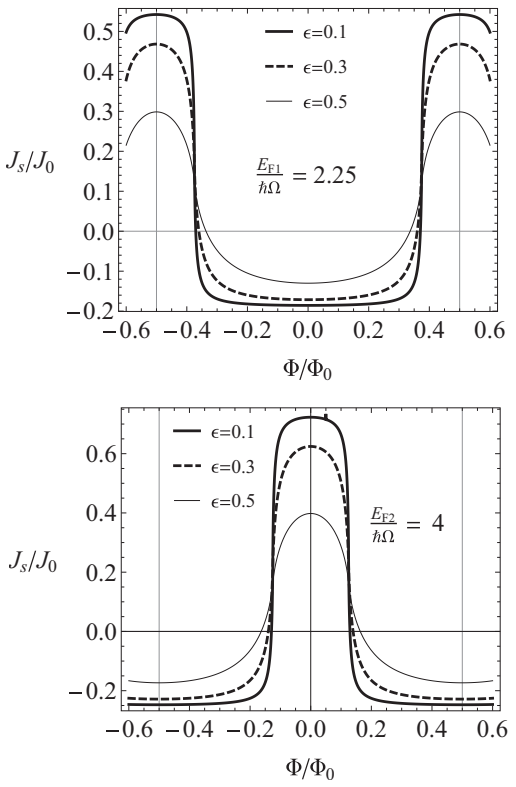

FIG. 10. Spin persistent current as a function of the magnetic flux for three values of ε and $T = 0$. The number of electrons is 6 (top) and 8 (bottom). The RSO is $\omega_{SO}/\Omega = 0.75$. The current is given in units of $J_0 = \hbar\Omega/\Phi_0$.

and the spin operator [24,31,35]

$$J_s^z = \frac{\hbar}{4}\Psi^\dagger\{\sigma_z, v_\varphi\}\Psi.$$

Invoking the full wave function derived above for the coupled ring and the velocity operator in Eq. (25), one can derive the spin current as

$$J_s^z = -\varepsilon\hbar\Omega\sum_{m,\mu}\int\frac{dE}{\hbar\Omega}\frac{f(E)}{\pi\sqrt{\frac{E}{\hbar\Omega}}g^\mu}\sin^2\left(\pi n_m^\mu\right) \times\left[\left(n_m^\mu - \frac{\Phi}{\Phi_0}\right)\beta^\mu + \gamma^\mu\right], \quad (28)$$

with

$$\gamma^1 = \sin^2\frac{\theta}{2}; \quad \gamma^2 = -\cos^2\frac{\theta}{2},$$
$$\beta^1 = \cos\theta; \quad \beta^2 = 1.$$

Figure 10 depicts the spin persistent current as a function of the magnetic flux for the two Fermi levels considered in Fig. 1. Spin currents are only possible in the presence of SO coupling since spin degeneracy matches up identical contributions in charge current from opposite spins (see Fig. 1 top panel). In the presence of the SO coupling there is a breaking of spin degeneracy with preservation of the time-reversal symmetry, the necessary ingredients for their presence. As for charge currents, spin currents from deep levels in the Fermi sea also tend to cancel but in a more

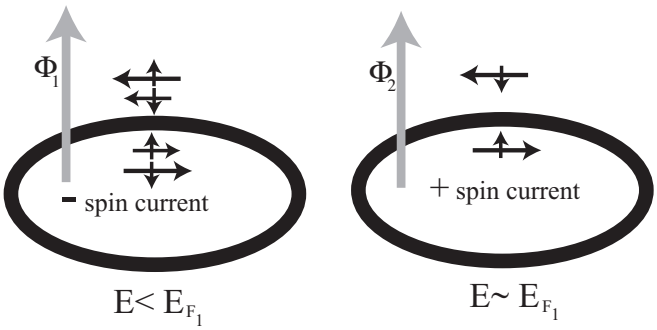

FIG. 11. The figure depicts, qualitatively, the contributions to the spin current as the flux changes until the Fermi level is reached. On the left, the currents in each direction are highly compensated in spin (each current direction contains both spin directions). On the right, the flux is such that the energy is close to the Fermi level E_{F_1}, and the spin current is large and switches direction.

complicated fashion. Figure 11 shows the combinations of charge currents with their corresponding spin orientations for the first Fermi-level scenario: Deep in the Fermi sea, charge currents are also paired up in spin but with small differences in electron velocities due to the broken degeneracy. So, we can see a small spin current accrued coming from these levels. As one goes higher in magnetic field, the positive current levels slow down, making less of a contribution, while the levels with negative charge currents speed up, making the bulk of

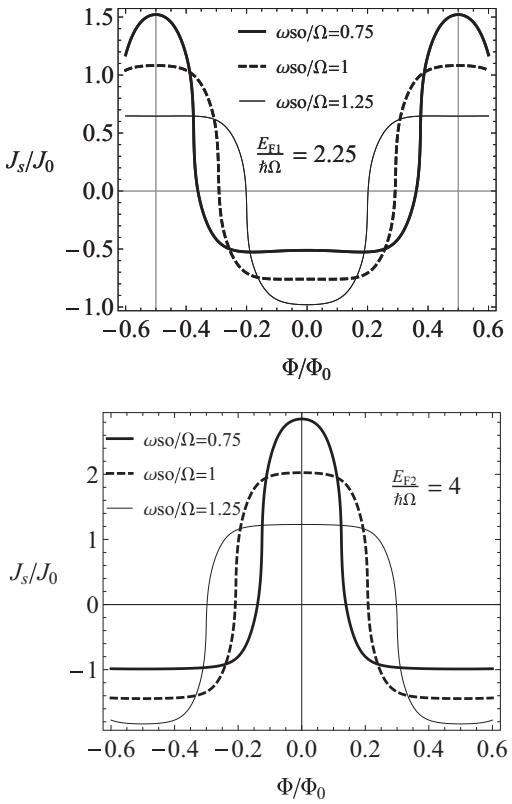

FIG. 12. Spin persistent current as a function of the magnetic flux for three values of ω_{SO}/Ω with finite temperature, $T/T_0 = 0.1$, and $\epsilon = 0.1$. The number of electrons is 6 (top) and 8 (bottom).

the current. The dispersion being quadratic makes for precise compensation, so that the full spin current is constant.

When the flux is large enough for the levels to cross the Fermi level, there is an abrupt disappearance of the negative spin-up current and a new contribution from a positive spin-up charge current, as shown in Fig. 11 right panel. These two contributions make for a pure spin current, more than three times the magnitude of the previous regime, very close to the Fermi level E_{F_1}. The range of fluxes in which this happens is as wide as it takes for the second level to emerge from the Fermi sea, i.e., $\Delta(\Phi/\Phi_0) = \sqrt{1+(\omega_{SO}/\Omega)^2} - 1$, at which point we restart with the scenario on the left panel and repeat the whole periodic oscillation.

For the second Fermi level, the scenario is similar but it occurs for small fluxes in the center of the spectrum (Fig. 10 bottom panel). Figure 12 shows how the spin currents, coming from different parts of the spectrum explored by the magnetic flux, can be tuned by the spin-orbit interaction at fixed coupling to the reservoir. One can see how positive and negative spin currents can be enhanced and change the range of fluxes for which they arise. It is interesting to note that the smaller spin current coming from levels deeper in the Fermi sea is more robust to decoherence (affected less by coupling to the reservoir) than the contributions coming from close to the Fermi level, resembling thermal effects previously discussed. On the other hand, as discussed for the charge currents, the Büttiker model is unable to completely degrade spin currents.

VI. SUMMARY AND CONCLUSIONS

The robustness of devices involving spin manipulation through the SO coupling against decoherence and thermal effects is crucial for their feasibility since these effects are unavoidable in practical applications. The latter, with the current lithographic techniques, always involve voltage gates, contacts with external reservoirs, and temperature points of operation which should not compromise the spin-sensitive physics of the device. With this concern in mind, we have solved for a generalization of the Büttiker voltage-probe model in SO active rings threaded by a magnetic flux. The procedure involves the determination of a complete set of basis functions for the uncoupled, phase-coherent, problem and then relaxing the quantization conditions on the closing of the wave functions when the scattering conditions are met at the reservoir junction. The coupling to the reservoir is spin insensitive and the thermal effects only determine the electron filling of the ring and did not induce additional broadening of the energy levels.

Complete analytical expressions for the density of states are obtained as a function of energy, magnetic flux, and SO coupling. As expected, the isolated ring levels broaden, and they do so in an energy-dependent fashion as the reservoir couples optimally at its own Fermi energy. We note that broadening effects are only Lorentzian for weak coupling to the reservoir, thus, our results contemplate strong reservoir coupling regime.

The equilibrium charge currents and spin currents were computed as sensitive probes for the action of both reservoir coupling and thermal effects. The linear-response formula to derive such currents is not directly useful in this case since the energy levels broaden into a continuum, so the quantum mechanical definitions were used with the full knowledge of the wave functions derived from the analytical procedure. Note that the full knowledge of the wave function for all reservoir couplings implies that, with the model reservoir, there is no loss of information that would entail a density-matrix description. Instead, the dephasing resulting in level broadening is derived from separating the ring and the reservoir lead wave functions (a kind of post-selection), where the DOS only involves the ring amplitudes containing part of the full wave function.

We computed the equilibrium charge and spin currents in the SO active ring coupled to the reservoir and assessed their coupling dependence to the electron reservoir and the effect of thermal occupation. Two representative Fermi-level scenarios were considered that involved where the spin-split structure of the spectrum is critical, i.e., close to multiples of $\Phi_0/2$. At those points, the sawtooth oscillating equilibrium current can be best modulated by the SO coupling strength. Experimentally feasible values for the SO strength were used in the computations.

While the coupling to the reservoir uniformly degraded the coherent currents, the thermal effects [36] revealed the interesting feature that there exist certain flux ranges that are protected by an energy-dispersion-dependent gap to the Fermi energy. This gap can be tailored by fixing the Fermi level and or the field flux. The magnitude of these protected currents is spectrum dependent but promises tailoring by considering more detailed models accounting for ring thickness and edge effects [37]. Equilibrium spin currents are obtained in steplike ranges in flux only for Rashba spin-orbit active material. The currents' steps are also rounded by coupling to the reservoir and temperature effects. Nevertheless, as these currents are built from charge currents distinguished in spin, so they are endowed with the same protective gaps. Therefore, there is a range of fluxes where spin currents are thermally protected. We expect the phenomena borne out from our model to be readily checked and exploited experimentally using recent techniques such as cantilever torsional magnetometry [38].

ACKNOWLEDGMENTS

N.B. thanks the Collège Doctoral Franco-Allemand 02-07 "Physics of Complex Systems" for financial support. E.M. and B.B. are respectively grateful to the University of Lorraine and to IVIC for invitations. They also thank the CNRS for support through the "PICS" programme *Spin transport and spin manipulations in condensed matter: polarization, spin currents and entanglement*. E.M. acknowledges support from Fundación POLAR. We thank an anonymous referee for suggesting the perturbative treatment of the reservoir coupling.

[1] R. Winkler, *Spin-Orbit Coupling Effects in Two Dimensional Electron and Hole Systems* (Springer, Berlin, 2003).

[2] J. R. Petta *et al.*, Science **309**, 2180 (2005).

[3] A. V. Khaetskii, D. Loss, and L. Glazman, Phys. Rev. Lett. **88**, 186802 (2002).

[4] F. E. Meijer, A. F. Morpurgo, and T. M. Klapwijk, Phys. Rev. B **66**, 033107 (2002).
[5] J. Nitta, F. E. Meijer, and H. Takayanagi, Appl. Phys. Lett. **75**, 695 (1999).
[6] M. Z. Hasan and C. L. Kane, Rev. Mod. Phys. **82**, 3045 (2010).
[7] J. Splettstoesser, M. Governale, and U. Zülicke, Phys Rev. B **68**, 165341 (2003).
[8] D. Frustaglia and K. Richter, Phys. Rev. B **69**, 235310 (2004).
[9] R. Ionicioiu and I. DÕAmico, Phys. Rev. B **67**, 041307(R) (2003).
[10] N. Hatano, R. Shirasaki, and H. Nakamura, Phys. Rev. A **75**, 032107 (2007); B. Santos, E. Medina, A. Lopez, and B. Berche, J. Appl. Phys. **110**, 114523 (2011).
[11] Duan-Yang Liu, and Jian-Bai Xia, J. Appl. Phys. **115**, 044313 (2014).
[12] M. Nita, D. C. Marinescu, A. Manolescu, and V. Gudmundsson, Phys. Rev. B **83**, 155427 (2011); M. Nita, D. C. Marinescu, A. Manolescu, B. Ostahie, and V. Gudmundsson, Phys. E (Amsterdam) **46**, 12 (2012).
[13] Y. S. Dedkov, M. Fonin, U. Rudiger, and C. Laubschat, Phys. Rev. Lett. **100**, 107602 (2008); M. Zarea and N. Sandler, Phys. Rev. B **79**, 165442 (2009).
[14] D. Marchenko, A. Varykhalov, M. R. Scholz, G. Bihlmayer, E. I. Rashba, A. Rybkin, A. M. Shikin, and O. Rader, Nat. Commun. **3**, 1232 (2012).
[15] M. Büttiker, Phys. Rev. B. **32**, 1846 (1985); IBM J. Res. Dev. **32**, 63 (1988).
[16] T. P. Pareek, S. K. Joshi, and A. M. Jayannavar, Phys. Rev. B **57**, 8809 (1998).
[17] E. Y. Tsymbal, V. M. Burlakov, and I. I. Oleinik, Phys. Rev. B **66**, 073201 (2002).
[18] Xin-Qi Li and YiJing Yan, Phys. Rev. B **65**, 155326 (2002).
[19] R. Golizadeh-Mojarad and S. Datta, Phys. Rev. B **75**, 081301 (2007).
[20] J. S. Sheng and K. Chang, Phys. Rev. B **74**, 235315 (2006).
[21] V. A. Margulis and V. A. Mironov, Phys. E (Amsterdam) **43**, 905 (2011).
[22] S. K. Maiti, M. Dey, S. Sil, A. Chakravarti, and S. N. Karmakar, Europhys. Lett. **95**, 57008 (2011).
[23] Y.-C. Zhou, H.-Z. Li, and X. Xue, Phys. Rev. B **49**, 14010 (1994).
[24] B. Berche, C. Chatelain, and E. Medina, Eur. J. Phys. **31**, 1267 (2010).
[25] Y.-S. Yi, T.-Z. Qian, and Z.-B. Su, Phys. Rev. B **55**, 10631 (1997).
[26] N. Bolívar, E. Medina, and B. Berche, Phys. Rev. B **89**, 125413 (2014).
[27] H. Förster, P. Samuelsson, S. Pilgram, and M. Büttiker, Phys. Rev. B **75**, 035340 (2007).
[28] M. Büttiker, Y. Imry, and M. Ya. Azbel, Phys. Rev. A **30**, 1982 (1984).
[29] H. M. Pastawski and E. Medina, Rev. Mex. Fis. **47 S1**, 1 (2001).
[30] S. Datta and B. Das, Appl. Phys. Lett. **56**, 665 (1990).
[31] S. Oh and C. M. Ryu, Phys. Rev. B. **51**, 13441 (1995).
[32] U. Ekenberg and D. M. Gvozdic, Phys. Rev. B **78**, 205317 (2008).
[33] D. Gosálbez-Martínez, D. Soriano, J. J. Palacios, and J. Fernándes Rossier, Solid State Commun. **152**, 1469 (2012).
[34] A. C. Bleszynski-Jayich, W. E. Shanks, and J. G. E. Harris, Appl. Phys. Lett. **92**, 013123 (2008).
[35] B. Molnár, F. M. Peeters, and P. Vasilopoulos, Phys. Rev. B **69**, 155335 (2004).
[36] Another nontrivial thermal effect due to peculiarities of the spectrum is reported in M. V. Moskalets and P. S. Deo, Phys. Rev. B **62**, 6920 (2000).
[37] J. A. M. van Ostaay, A. R. Akhmerov, C. W. J. Beenakker, and M. Wimmer, Phys. Rev. B **84**, 195434 (2011).
[38] A. C. Bleszynski-Jayich, W. E. Shanks, B. R. Ilic, and J. G. E. Harris, J. Vac. Sci. Technol. B **26**, 1412 (2008).